Origin of transverse magnetization in epitaxial Cu/Ni/Cu nanowire arrays

M. Ciria,[1,2,*] F. J. Castaño,[3] J. L. Diez-Ferrer,[2,4] J. I. Arnaudas,[2,4] B. G. Ng,[3] R. C. O'Handley,[3] and C. A. Ross[3]
[1]*Departamento de Magnetismo de Sólidos, Instituto de Ciencia de Materiales de Aragón, Consejo Superior de Investigaciones Científicas, 50009 Zaragoza, Spain*
[2]*Departamento de Física de la Materia Condensada, Universidad de Zaragoza, 50009 Zaragoza, Spain*
[3]*Department of Materials Science and Engineering, Massachusetts Institute of Technology, Cambridge, Massachusetts 02139, USA*
[4]*Instituto de Nanociencia de Aragón, Universidad de Zaragoza, 50009 Zaragoza, Spain*
(Received 3 April 2009; revised manuscript received 17 July 2009; published 24 September 2009)

The patterning-induced changes in the magnetic anisotropy and hysteresis of epitaxial (100)-oriented Cu/Ni(9, 10, 15 nm)/Cu planar nanowires have been quantified. When the Ni films are patterned into lines, strain relaxation leads to a thickness-dependent net in-plane anisotropy transverse to the lines. The magnetoelastic anisotropy was found from the three-dimensional strain state measured directly by synchrotron x-ray diffraction and has a value of -21 kJ/m^3 for 10-nm-thick nanowires. The angular dependence of the remanence of the nanowires indicates that the in-plane easy direction is the result of the competition between the cubic magnetocrystalline anisotropy and a uniaxial anisotropy that includes shape and magnetoelastic effects. The patterning-induced changes in magnetoelastic anisotropy, combined with the shape and magnetocrystalline anisotropies, quantitatively explain the net anisotropy of the nanowires. Thus by controlling the film thickness and wire orientation, the easy axis direction of the nanowires may be controlled.

DOI: 10.1103/PhysRevB.80.094417 PACS number(s): 75.30.Gw, 75.50.Cc, 75.75.+a

I. INTRODUCTION

The control of the magnetic anisotropy and domain configurations in lithographically defined magnetic elements with submicron lateral dimensions is of importance for spintronic devices. Planar nanowires (NWs), in particular, have been investigated because of their potential use in domain-wall devices proposed for data storage[1] and logic applications.[2] Most reported work has been focused on nanowires patterned from polycrystalline films, whose properties are dominated by shape anisotropy, and which exhibit domains with the magnetization pointing along the wire axis separated by either transverse or vortexlike 180° head-to-head domain walls (DWs).[3] However, materials with different domain states and DW geometries could offer advantages in spintronic applications, for example, metallic planar NWs with perpendicular magnetic anisotropy exhibit current-induced DW motion at lower threshold current values compared to those of NWs with in-plane anisotropy.[4,5] Therefore, developing methods for tuning the magnetic anisotropy of NWs may offer new opportunities for spintronic devices.

The magnitude and direction of the net anisotropy determine the domain structure and the DW type of a patterned element. Anisotropy is most commonly controlled via the geometrical shape of the structure,[6] or by magnetocrystalline anisotropy,[7] but in certain strained epitaxial magnetic films, magnetoelastic (ME) effects can dominate the anisotropy,[8–10] leading, for example, to a net anisotropy K_p oriented perpendicular to the film plane. Patterning of a strained layer breaks the in-plane symmetry and produces an asymmetric strain relaxation and an in-plane ME anisotropy contribution to the total magnetic anisotropy energy.

The in-plane anisotropy energy of a NW made from a single-crystal cubic material includes the magnetocrystalline anisotropy $K_1 \cos^2\phi \sin^2\phi$ plus the ME and magnetostatic contributions $(K_{me}+K_{sh})\sin^2\phi$, a uniaxial term, where ϕ is the angle between the magnetization M and the NW axis. The shape energy term can be written as $K_{sh}=0.5\ \mu_0 (N_y-N_x)M^2$ (we assign $x\|$NW axis and $y\perp$NW axis, thus N_y and N_x are, respectively, the transverse and longitudinal demagnetization factors). Because K_{sh} is always positive (giving an easy direction along the NW axis), the in-plane uniaxial anisotropy term will depend on the sign of the ME coefficient K_{me}. If $K_{me}>0$ the uniaxial anisotropy along the NW is enhanced, as observed in magnetic semiconductors such as (Ga,Mn)As/(In,Ga)As,[11] while if $K_{sh}<-K_{me}$ the uniaxial anisotropy drives M transverse to the NW axis. For cubic thin-film materials grown on the (001) plane, $K_{me}=-B_1\epsilon_\gamma$, where B_1 is the ME stress coefficient and $\epsilon_\gamma=\epsilon_{xx}-\epsilon_{yy}$ is the strain associated with the breaking of the in-plane fourfold symmetry. The sign of ϵ_γ in a patterned heteroepitaxial system can be obtained by considering two factors: first, the strain relaxation in a NW is larger along the direction transverse to the NW axis so $|\epsilon_{xx}|>|\epsilon_{yy}|$ and second, the misfit between the substrate lattice parameter a_s and the lattice parameter of the magnetic material a_m determines the sign of ϵ_{xx} and ϵ_{yy}, so that $a_m>(<)a_s \Rightarrow \epsilon_{xx},\ \epsilon_{yy}<(>)0$ and $\epsilon_\gamma<(>)0$. The Ni/Cu(001) system, which has $B_1>0$ and $a_{\mathrm{Ni}}<a_{\mathrm{Cu}}$, can meet the criterion $-K_{me}=B_1\epsilon_\gamma>K_{sh}$ and is therefore able to produce NWs with magnetization in-plane but transverse to the wire axis. We have shown previously that patterning Cu/Ni/Cu(001) epitaxial films of 6.9 and 20.6 nm Ni thickness can indeed lead to NWs with a net transverse anisotropy.[12]

In the present work we demonstrate, by measuring the in-plane lattice parameters and determining ϵ_γ, that the transverse anisotropy observed in NW arrays of patterned epitaxial Cu/Ni/Cu films with nickel thickness $t_{\mathrm{Ni}}=9$, 10, and 15 nm, is due to a K_{me} that is large enough to overcome K_{sh}. We show that the easiest in-plane direction forms an angle with the NW axis that depends on the ratio K_1/K_u, with K_1 the cubic magnetocrystalline anisotropy constant and $K_u=(K_{me}+K_{sh})\sin^2\phi$, the uniaxial term including ME and

 ©2009 The American Physical Society

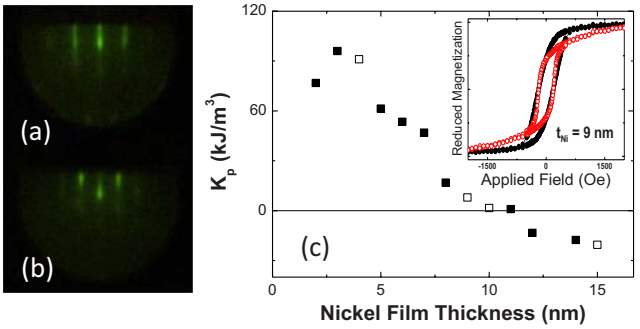

FIG. 1. (Color online) RHEED pattern of the (a) [100] and (b) [110] Ni azimuth directions. (c) K_p vs t_{Ni} for the samples in this study. The films that were later patterned are indicated by the open symbols. The inset shows M-H loops for the 9-nm-thick film with a field applied parallel (○) and perpendicular (●) to the plane. The field range of the measurement is ±15 kOe.

shape anisotropy. K_1 favors magnetization along the in-plane ⟨110⟩ directions and K_u favors anisotropy transverse to the NW axis. Thus, the combination of competing anisotropies suggests a way to engineer NWs with controlled easy magnetization direction.

II. EXPERIMENTAL METHODS

Epitaxial Cu (5 nm)/Ni (t_{Ni})/Cu (100 nm) films with t_{Ni} between 2 and 15 nm were grown on Si (001) wafers at room temperature by electron-beam evaporation in a chamber with a base pressure below 2×10^{-10} Torr, using a procedure reported elsewhere.[13] The single-crystal nature of each layer and the epitaxial relationships, i.e., Si⟨100⟩ ‖Cu⟨110⟩‖ Ni⟨110⟩, are observed *in situ* by reflection high-energy electron diffraction (RHEED), see Figs. 1(a) and 1(b), and high-resolution grazing incidence x-ray diffraction (XRD), done in the BM25B beamline of ESRF using a photon energy of $h\nu=15$ keV. The magnetic properties of the samples were investigated by alternating gradient magnetometry, vibrating sample magnetometry, and magnetic force microscopy (MFM), using a low-moment tip. In addition to the anisotropy calculation based on strain, an estimate of the effective magnetic anisotropy constants was also made from the difference between magnetization loops measured along specific directions.[10] To eliminate the effect of hysteresis, the anhysteretic M-H curve is calculated by averaging the descending and ascending branches of the hysteresis loop at constant values of M. Arrays of Cu/Ni/Cu nanowires with the wire axis along the Ni ⟨100⟩ direction were fabricated by ion-beam etching (see Fig. 2), using a Ta grating as a hard

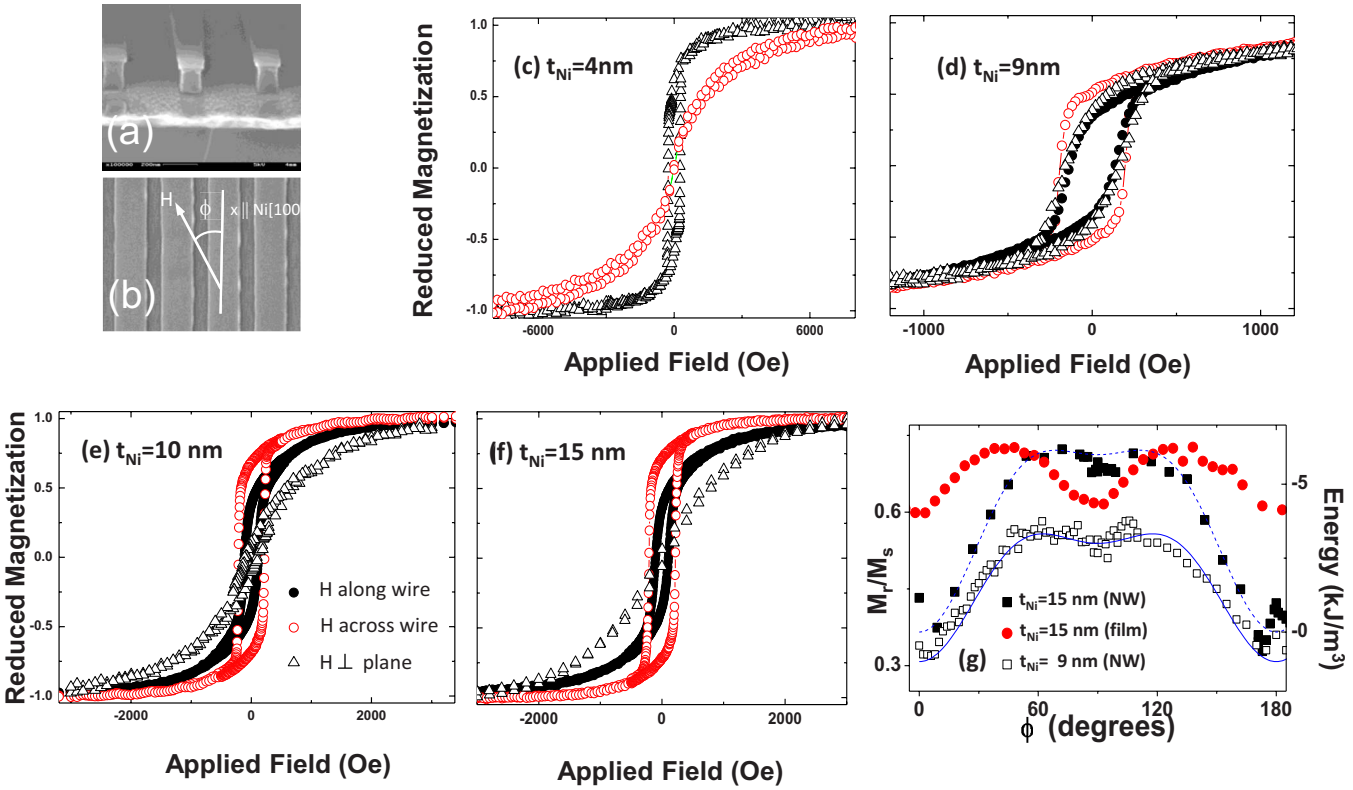

FIG. 2. (Color online) (a) SEM images of grating pattern of resist on the magnetic films and (b) NW sample after hard mask deposition and ion-beam etching. $M(h)$ loops for NW arrays with nickel thickness equal to (c) 4, (d) 9, (e) 10, (f) 15 nm. Triangles indicate $H\perp$ to the film plane, open circles correspond to H transverse to the NW axis and full symbols indicate $H\|$NW array. For the 4NW sample the two in-plane loops are equivalent and only one loop is represented; (g) angular variation in M_r/M_s for the 15NW (solid squares), and the 9NW (empty squares) arrays and the 15-nm-thick film (circles); the dashed line is $E_{anis}(\phi)$ with $K_u=-6$ kJ/m^3 and $K_1=-10$ kJ/m^3 and the continuous line is $E_{anis}(\phi)$ with $K_u=-4$ kJ/m^3 and $K_1=-7$ kJ/m^3 shifted by a constant value to fall on the 9NW data.

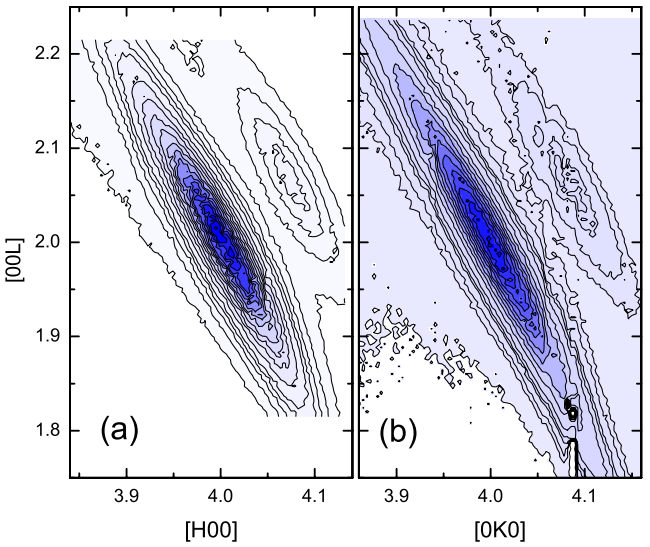

FIG. 3. (Color online) Reciprocal space maps taken for the 10NW array along (a) the [402] and (b) the [042] directions of copper and nickel. Units of the scattering vector both parallel and perpendicular to the sample surface are related to the primitive cell of the bulk copper.

mask. The Ta was patterned using interference lithography[14] and reactive ion etching to form a polymer grating from a trilayer resist stack, then sputtering and liftoff of Ta to form the hard mask. We fabricated four NW arrays with t_{Ni}=4, 9, 10, and 15 nm, which will be labeled as 4NW, 9NW, 10NW, and 15NW, respectively. Samples 9NW, 10NW, and 15NW have a period close to 450 nm and a wire width of 300, 200 and 200 nm, respectively, while 4NW had a period of 800 nm and a wire width of 600 nm.

III. RESULTS AND DISCUSSION

Magnetometry shows that the unpatterned nickel films exhibit out-of-plane magnetization, with an effective perpendicular magnetic anisotropy $K_p>0$, for t_{Ni} between about 1.5 and 11.5 nm [see Fig. 1(c)], in agreement with other work.[8,9] The 4-, 9-, and 10-nm-thick films are more easily magnetized out-of-plane compared to in-plane ($K_p>0$) while for the 15 nm film the opposite behavior is observed ($K_p<0$).

Figure 2 shows data for the patterned films. The in-plane loops with H applied along the x and y directions provide information about the effects of patterning on the magnetic behavior. These samples span the range from high K_p (t_{Ni}=4 nm) to a regime (t_{Ni}=9, 10, and 15 nm) where K_p is low and its sign changes from positive to negative. For 4NW, K_p is positive, while for 9NW, 10NW, and 15NW, K_p is negative, showing that K_p has changed sign for t_{Ni}=9 and 10 nm. For the three samples with negative K_p the hysteresis loops suggest that M is oriented preferentially in plane, transverse to the nanowires, particularly for the 10NW and 15NW samples. This result, which is consistent with our prior work,[12] is contrary to what would be expected from shape anisotropy alone, and demonstrates the governing effect of K_{me}.

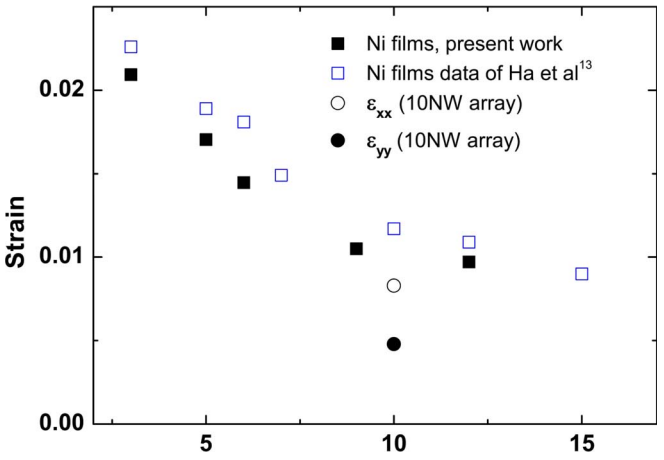

FIG. 4. (Color online) In-plane strain for the 10NW array longitudinal (empty circle) and transverse to the NW axis (full circle) and for two series of nickel films: the films used to fabricate the NW arrays (full squares), and data extracted from Ref. 13 (empty squares).

A direct measurement of the strain asymmetry is required to quantify the ME anisotropy. This was performed for sample 10NW. The strain state in the 10NW array was determined from XRD reciprocal space mapping in the vicinity of the asymmetric (402) and (042) Bragg reflection from Cu and Ni layers (see Fig. 3). These scans are sensitive to the lattice parameter a_x parallel to the NW axis [see Fig. 3(a)] and a_y transverse to the NW axis [see Fig. 3(b)], as well as to the out-of-plane lattice parameter.[15] These scans show both Ni and Cu reflections, and while the copper peak is at the bulk value (units in Fig. 3 are related to the bulk copper lattice parameter) the nickel peak positions are both shifted with respect to the bulk value and by about 0.15 units with respect to each other. From the experimental positions of the maxima of the scattered intensity the in-plane lattice constants were determined as a_x=3.553 Å, a_y=3.541 Å, and a_z=3.504 Å leading to $\epsilon_{xx}=(8.3\pm0.1)\times10^{-3}$, $\epsilon_{yy}=(4.9\pm0.1)\times10^{-3}$, and $\epsilon_{zz}=(-5.7\pm0.1)\times10^{-3}$, respectively. Figure 4 gives a comparison between these in-plane strain components and those obtained for a series of unpatterned films measured in the same diffractometer by grazing incidence XRD, as well as data reported elsewhere.[13] The ϵ_{xx} of the 10NW sample is close to the value found for the unpatterned films while ϵ_{yy} is about half as large, indicating that the nanowires undergo a relaxation transverse to the NW axis. Considering the z direction, ϵ_{zz} is smaller than the value $\epsilon_{zz}\approx-12.8\times10^{-3}$ calculated for the biaxially stressed unpatterned film ($\epsilon_{zz}=-2(c_{12}/c_{11})\epsilon_{xx}$, where the c's are the nickel elastic constants and $\epsilon_{xx}\approx-10\times10^{-3}$),[13] showing that ϵ_{zz} is also relaxed in the NW array.

Based on $\epsilon_\gamma=\epsilon_{xx}-\epsilon_{yy}\approx(3.4\pm0.2)\times10^{-3}$ for sample 10NW, we obtain $K_{me}=-21\pm2$ kJ/m^3 [with B_1=6.2 MPa (Ref. 16)]. K_{sh} was determined by using the demagnetizing factors for arrays of planar NWs reported in Ref. 17. With N_x=0 and $N_y=0.91t_{Ni}/w$ (w=width) for the array, a value slightly smaller than that of a single infinite NW, K_{sh}=6.6 kJ/m^3 for sample 10NW. These values imply K_u=−14.4 kJ/m^3 which quantifies the transverse anisotropy

in terms of a ME effect due to asymmetrical relaxation of the in-plane epitaxial lattice strain.

An estimate of K_u may also be obtained from the anhysteretic M-H curves measured in the longitudinal and transverse directions.[10] This yields K_u (15NW)=−6.0 kJ/m^3; K_u (10NW)=−6.3 kJ/m^3, and K_u (9NW)=−4.0 kJ/m^3. The value for 10NW is in reasonable agreement with that calculated from the measurement of the strain, considering the approximations of the estimate based on hysteresis. The NWs were patterned such that the ⟨100⟩ in-plane directions are parallel to the NW axis, and the ⟨110⟩ in-plane directions, which are magnetically easy according to the magnetocrystalline anisotropy, form an angle of 45° to the NW axis. Thus, a competition between the uniaxial term and the magnetocrystalline contribution is expected. To elucidate that competition we examine the symmetry of the in-plane magnetic anisotropy. Figure 2(g) presents the variation in the remanence ratio M_r/M_s as function of the angle ϕ between the NW axis (x axis) and H for the 9NW and 15NW arrays and for the 15 nm unpatterned film, in which ϕ=0 corresponds to a ⟨100⟩ direction. As expected, for the unpatterned film, M_r/M_s displays a fourfold dependence on ϕ. The ⟨110⟩ directions, at 45° to the NW axis, are the in-plane easy axes. M_r/M_s takes maximum and minimum values along the ⟨110⟩ easy and ⟨100⟩ hard axes, respectively, defined by the magnetocrystalline anisotropy $K_1 \cos^2\phi \sin^2\phi$ with K_1=−4.5 kJ/m^3.[16]

For the 9NW and 10NW arrays the in-plane ⟨110⟩ direction is no longer the easy in-plane direction. Instead, the maximum values of M_r/M_s are near ϕ=70°, although the difference between the values for M_r/M_s at ϕ=70° and 90° is small. The minimum value for M_r/M_s is at ϕ=0°. In the (001) plane, the total anisotropy energy E_{anis} can be modeled as the sum of a uniaxial term, comprising shape and ME contributions, and the magnetocrystalline contribution: $E_{anis}(\phi)=K_u \sin^2\phi+K_1 \cos^2\phi \sin^2\phi$. The minimum for $E_{anis}(\phi)$ depends on the K_u/K_1 ratio. If both constants are negative, for $|K_u|>|K_1|$ the minimum is at 90°, whereas if $|K_u|<|K_1|$ the minimum is given by $\cos 2\phi=-K_u/K_1$.

Taking the value at which M_r/M_s has its maximum value as the minimum of $E_{anis}(\phi)$ and using the value of K_u obtained from hysteresis loops and strain data, we obtain, $K_1 \sim -7.5$ and −18.4 kJ/m^3, respectively, for sample 10NW. This suggests that K_1 is greater than the magnetocrystalline anisotropy of bulk Ni, which is −4.5 kJ/m^3. An enhancement of K_1 in nickel thin films has been reported[18,19] and its origin linked to a magnetoelastic contribution due to the isotropic in-plane stress in the film arising from the misfit between substrate and film. The lines in Fig. 2(g) represent $E_{anis}(\phi)$ calculated for the 9NW and 15NW arrays, and show excellent agreement with the measured angular dependence of the ratio M_r/M_s indicating the presence of a uniaxial term in E_{anis}.

Magnetic force microscopy was used to clarify the domain structure and aid in the interpretation of the anisotropy data. Figure 5 shows images of samples 4NW and 9NW. For 4NW, comparing images taken in the same area, in the remanent state [Fig. 5(a)] after out-of-plane saturation the Ni NWs show all-bright magnetic contrast, indicating a high remanence consistent with the hysteresis loop, while the out-of-plane ac-demagnetized state [Fig. 5(b)] shows dark and bright domains along the wires with lengths of 1–10 μm, much longer than the wire width or thickness. For sample 9NW, Fig. 5(c), taken also in a out-of-plane ac-demagnetized state, the domain configuration is more complicated and a few μm long domains are visible with dark and light contrasts. Using dust particles that induce a topography signal for reference, see Fig. 5(d), we observe that the maximum magnetic contrast corresponds to near the edges of the topography, and is consistent with a magnetization transverse to the wire length, as suggested by the hysteresis loops. A simple model supports the qualitative analysis of the MFM images: the strength of the z component of the fringing field as function of y for an infinite planar nanowire with uniform magnetization confined in the y-z plane transverse to the wire axis is calculated[16] as a function of the angle γ between

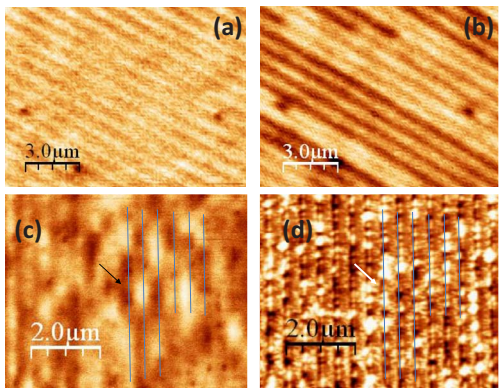

FIG. 5. (Color online) (a) and (b) MFM images of sample 4NW after (a) out-of-plane saturation, (b) out-of-plane ac demagnetization. These images cover the same sample area, as indicated by the positions of the three dark defect spots. (c) Magnetic and (d) topographic images of sample 9NW after out-of-plane ac demagnetization. The arrows indicate particles used as reference. The continuous lines indicate the spaces between Ni NWs.

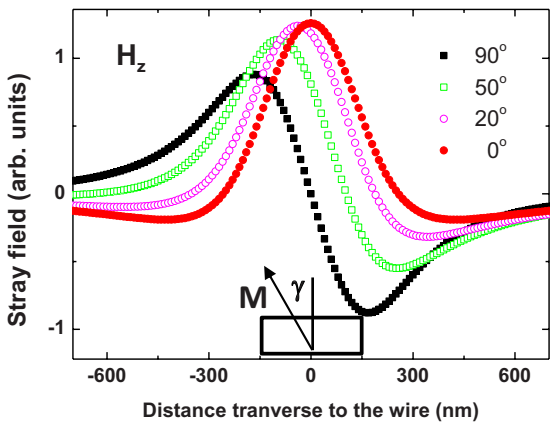

FIG. 6. (Color online) Vertical component H_z of the stray field at z=225 nm as a function of the distance y transverse to the NW axis and angle γ (=0°, 20°, 50°i, and 90°). The field is generated by an infinite planar nanowire with uniform magnetization confined in the plane perpendicular to the wire axis. γ is the angle between the magnetic moment and the z direction. The wire is 250 nm wide and 10 nm thick.

M and the z direction, Fig. 6. For $\gamma=0$, the stray field is maximum in the nanowire center, as is observed for 4NW, while if γ increases, the extremal values move toward the NW edge as seen for 9NW.

Finally, we reconsider the strain data to show why K_p decreases on patterning: K_p includes the ME term $-B_1[\epsilon_{zz}-0.5(\epsilon_{xx}+\epsilon_{yy})]$ and the components of strain decrease on patterning. For an unpatterned Ni film in biaxial stress, the ME contribution to anisotropy reduces to $B_1\epsilon_{xx}[1+2(c_{12}/c_{11})]$, with $B_1=6.2$ MPa and the ratio $c_{12}/c_{11}=0.64$. This gives a value for the ME contribution of 141 $\mathrm{kJ/m^3}$ for the 10-nm-thick film in which $\epsilon_{xx}=0.01$. For the 10NW sample, we use for the strain components the values measured by x-ray diffraction. We find that the ME contribution to K_p is 76 $\mathrm{kJ/m^3}$, showing that K_p must have decreased by about 65 $\mathrm{kJ/m^3}$ upon patterning. This decrease is larger than the net K_p of the unpatterned film, which was about 10 $\mathrm{kJ/m^3}$. This explains why K_p becomes negative in the 9 and 10-nm-thick patterned NWs despite being positive for the unpatterned films. In contrast, for the 4-nm-thick sample, the K_p of the unpatterned film was about 90 $\mathrm{kJ/m^3}$ so the strain relaxation is insufficient to drive the net anisotropy in plane, and the patterned 4NW sample retains its out-of-plane anisotropy.

IV. SUMMARY

We have quantitatively analyzed the magnetoelastic, shape and magnetocrystalline anisotropies for planar nanowire arrays made from heteroepitaxial Cu/Ni/Cu thin films with a range of Ni film thicknesses. Patterning the continuous films leads to anisotropic stress relief and a magnetoelastic anisotropy which can dominate the net magnetic anisotropy of the Ni nanostructures. These results show how magnetoelastic effects may be used to control the net anisotropy and magnetic properties of patterned nanostructures, leading, for example, to nanomagnets with tailored in-plane magnetic anisotropy.

ACKNOWLEDGMENTS

We thank B. Pita, V. García, and F. Ilievski for their help in this work. We acknowledge the European Synchrotron Radiation Facility for provision of synchrotron radiation facilities and we would like to thank the staff at Spline for assistance in using beamline BM25. This work has been supported by Spanish MICINN (Grants No. MAT2006-07094, No. PI049/08, and No. NAN2004-09183-C10-10) and DGA (Grant No. E81) and Fondo Social Europeo and the Singapore-MIT Alliance.

*ciria@unizar.es

[1] S. S. Parkin, M. Hayashi, and L. Thomas, Science **320**, 190 (2008).
[2] D. A. Allwood, G. Xiong, C. C. Faulkner, D. Atkinson, D. Petit, and R. P. Cowburn, Science **309**, 1688 (2005).
[3] A. Hubert and R. Schafer, *Magnetic Domains: The Analysis of Magnetic Microstructures* (Springer, Berlin, 1998).
[4] D. Ravelosona, D. Lacour, J. A. Katine, B. D. Terris, and C. Chappert, Phys. Rev. Lett. **95**, 117203 (2005).
[5] S.-W. Jung, W. Kim, T.-D. Lee, K.-J Lee, and H.-W. Lee, Appl. Phys. Lett. **92**, 202508 (2008).
[6] P. Bruno, Phys. Rev. Lett. **83**, 2425 (1999).
[7] S. Cherifi, R. Hertel, A. Locatelli, Y. Watanabe, G. Potdevin, A. Ballestrazzi, M. Balboni, and S. Heund, Appl. Phys. Lett. **91**, 092502 (2007).
[8] R. Jungblut and M. T. Johnson, J. aan de Stegge, A. Reinders, and F. J. A. den Broeder, J. Appl. Phys. **75**, 6424 (1994).
[9] G. Bochi, C. A. Ballentine, H. E. Inglefield, C. V. Thompson, and R. C. O'Handley, Phys. Rev. B **53**, R1729 (1996).
[10] M. T. Johnson, P. J. H. Bloemen, F. J. A. den Broeder, and J. J. de Vries, Rep. Prog. Phys. **59**, 1409 (1996).
[11] J. Wenisch, C. Gould, L. Ebel, J. Storz, K. Pappert, M. J. Schmidt, C. Kumpf, G. Schmidt, K. Brunner, and L. W. Molenkamp, Phys. Rev. Lett. **99**, 077201 (2007).
[12] E. Lyons, R. C. O'Handley and C. A. Ross, J. Appl. Phys. **95**, 6711 (2004); **99**, 08R105 (2006).
[13] K. Ha, M. Ciria, R. C. O'Handley, P. W. Stephens, and S. Pagola, Phys. Rev. B **60**, 13780 (1999).
[14] H. I. Smith, Physica E (Amsterdam) **11**, 104 (2001).
[15] H. Heinke, S. Einfeldt, B. Kuhn-Heinrich, G. Plahl, M. O. Möller, and G. Landwehr, J. Phys. D **28**, A104 (1995).
[16] R. C. O'Handley, *Modern Magnetic Materials: Principles and Applications*, (John Wiley & Sons, 2000).
[17] B. B. Pant, J. Appl. Phys. **79**, 6123 (1996).
[18] S. Chikazumi, J. Appl. Phys. **32**, S81 (1961).
[19] J. F. Freedman, IBM J. Res. Dev. **6**, 442 (1962).